Stochastic Reduced Order Models For Uncertain Nonlinear Dynamical Systems

Marc P. Mignolet[1] and Christian Soize[2]

[1] Department of Mechanical and Aerospace Engineering
Arizona State University, Tempe, AZ 85287-6106, USA - Email: marc.mignolet@asu.edu
[2] Laboratoire de Mécanique, Université de Marne-La-Vallée
5, Bd Descartes, 77454 Marne-La-Vallée Cedex 02, France - E-mail: soize@univ-mlv.fr

ABSTRACT

A general methodology is presented for the consideration of both data and model uncertainty in the determination of the response of geometrically nonlinear structural dynamic systems. The approach is rooted in the availability of reduced order models of these nonlinear systems with a deterministic basis extracted from a reference model (the mean model). Uncertainty, both from data and model, is introduced by randomizing the coefficients of the reduced order model in a manner that guarantees the physical appropriateness of every realization of the reduced order model, i.e. while maintaining the fundamental properties of symmetry and positive definiteness of every such reduced order model. This randomization is achieved not by postulating a specific joint statistical distribution of the reduced order model coefficients but rather by deriving this distribution through the principle of maximization of the entropy constrained to satisfy the necessary symmetry and positive definiteness properties. Several desirable features of this approach are that the uncertainty can be characterized by a single measure of dispersion, affects all coefficients of the reduced order model, and is computationally easily achieved. The reduced order modeling strategy and this stochastic modeling of its coefficients are presented in details and several applications to a beam undergoing large displacement are presented. These applications demonstrate the appropriateness and computational efficiency of the method to the broad class of uncertain geometrically nonlinear dynamic systems.

INTRODUCTION

The need to include system uncertainty in dynamic analyses has long been recognized in the context of some specific problems. For example, the response of turbomachinery/engine bladed disks has been known since the late 1960's (e.g. [1]) to be highly sensitive to small blade-to-blade variations in their material/geometrical properties. This lack of robustness has thus motivated numerous stochastic analyses in which the uncertainty/variations in blade properties was introduced through the representation of certain blade characteristics as random variables. This stochastic modeling has however typically been ad-hoc, i.e. only some of the blade properties were considered as random, most notably natural frequencies, based on demonstrated/perceived sensitivity.

With predictive capabilities becoming always faster and allowing always more complex models, the limitations associated with the uncertainty in the *parameters of the system*s (data uncertainty, e.g. in the material properties) and in the *computational modeling* of the physical system (model uncertainty, e.g. in the finite element representation of fasteners, lap joints, etc. and the approximation of the physical geometry) now appear clearly in many areas of structural dynamics. Accordingly, it has become quite

important to dispose of *general* methodologies for the inclusion of uncertainty in dynamic analyses, as opposed to the ad-hoc approaches used in the past, and a series of recent investigations have focused on devising such general techniques that are consistent with state-of-the-art computational tools. An attractive approach of this type for data uncertainty is the stochastic finite element method (see in particular [2]) in which the random fields characterizing both the uncertain material properties and the response of the system are described by polynomial chaos expansions. Then, given a complete characterization of the uncertain material properties, a similarly complete representation of the stochastic response is obtained. Note however that this probabilistic approach relies on a *given computational model* and thus does not allow the consideration of model uncertainty.

A probabilistic approach that does include both data and model uncertainty has recently been devised (Soize, [3-5]) and applied/validated (see [6] for a review) on a variety of dynamic problems involving linear structures with possible additional local nonlinearities. The inclusion of data and model uncertainty is accomplished in reduced order models of the structure through an appropriate stochastic representation of the elements of its mass, damping, and stiffness matrices. The variations of these random matrices around a baseline model (referred to as the mean model) is characterized by a single measure of dispersion, as opposed to a large number of parameters from statistical distributions. Accordingly, this probabilistic approach has been referred to as nonparametric and thus exhibits the following advantageous properties:

    i) includes both model and data uncertainty,

    ii) is characterized by only a mean reduced order model and a measure of dispersion, and,

    iii) is computationally expedient because it relies on reduced order models for the Monte Carlo simulations typically involved in the stochastic analysis of uncertain systems.

These important properties motivate the extension of the nonparametric approach to dynamic systems with distributed, geometric nonlinearity, which is the focus of the present investigation. This extension will rely in particular on recent developments in the formulation of reduced order models of geometrically nonlinear systems (e.g. [7-10]) and will be accomplished in the general framework of linearly elastic geometrically nonlinear structures which encompasses as special cases beams and plates with the von Karman strain definition.

GEOMETRIC NONLINEAR FORMULATION

While many of the classical structural dynamic problems involving geometric nonlinearity relate to beam, plates, and shells in which the von Karman strain definition is used, it is of interest here to demonstrate the general applicability of the nonparametric stochastic modeling approach. To this end, an arbitrary linearly elastic (i.e. with a linear relation between the Green strain and second Piola-Kirchhoff stress tensors) structure undergoing large deformations will be considered in the sequel.

The position vector of a point of the structure will be denoted by $\underline{X}$ in the reference configuration and as $\underline{x}$ in the deformed one so that the displacement vector is $\underline{u} = \underline{x} - \underline{X}$. The deformation gradient tensor $\underline{\underline{F}}$ is then defined by its components F_{ij} as

$$F_{ij} = \frac{\partial x_i}{\partial X_j} = \delta_{ij} + \frac{\partial u_i}{\partial X_j} \tag{1}$$

where δ_{ij} denotes the Kronecker symbol. Associated with the displacement field $\underline{u}$ are deformations which are characterized by the Green strain tensor $\underline{\underline{E}}$ of components

$$E_{ij} = \frac{1}{2}\left(F_{ki}\,F_{kj} - \delta_{ij}\right). \tag{2}$$

Note in the above equation and in the ensuing ones that summation is implied on all repeated indices.

The equation of motion of the structure is then given by (e.g. see [11])

$$\frac{\partial}{\partial X_k}\left(F_{ij}\,S_{jk}\right) + \rho_0\,b_i^0 = \rho_0\,\ddot{u}_i \qquad \text{for } \underline{X} \in \Omega_0 \tag{3}$$

where $\underline{S}$ denotes the second Piola-Kirchhoff stress tensor, ρ_0 is the density in the reference configuration, and $\underline{b}^0$ is the vector of body forces, all of which are assumed to depend on the coordinates X_i and be expressed in the reference configuration in which the structure occupies the domain Ω_0. The boundary, $\partial\Omega_0$, of the reference configuration domain Ω_0, is composed of two parts, $\partial\Omega_0^t$ on which the tractions $\underline{t}^0$ are given and $\partial\Omega_0^u$ on which the displacements are specified. Accordingly, the boundary conditions are

$$F_{ij}\,S_{jk}\,n_k^0 = t_i^0 \qquad \text{for } \underline{X} \in \partial\Omega_0^t \tag{4}$$

and

$$\underline{u} = \underline{0} \qquad \text{for } \underline{X} \in \partial\Omega_0^u. \tag{5}$$

Note in Eqs (3) and (4) that the vectors $\underline{b}^0$ and $\underline{t}^0$ correspond to the transport of the body forces and tractions applied on the deformed configuration, i.e. $\underline{b}$ and $\underline{t}$, back to the reference configuration. This operation is accomplished through the relations

$$\underline{b}^0 = J\,\underline{b} \qquad \text{and} \qquad t_0 = \left(\frac{da}{dA}\right)t \tag{6}$$

where J is the Jacobian of the transformation $\underline{x} = \underline{x}(\underline{X})$, i.e. $J = \det(\underline{\underline{F}})$. Further, the area ratio da/dA can be expressed evaluated from [12]

$$\frac{da}{dA}\,\underline{n} = J\,\underline{\underline{F}}^{-T}\,\underline{N} \tag{7}$$

where $\underline{N}$ is the unit normal vector to $\partial\Omega_0$ at the boundary point $\underline{X}$ and $\underline{n}$ is its counterpart on the deformed configuration.

To complete the formulation of the elastodynamic problem, it remains to specify the constitutive behavior of the material. In this regard, it will be assumed here that the structure may exhibit a given nonzero steady temperature distribution $T(\underline{X})$. Then, adopting a linear elastic model between the Green strain and second Piola-Kirchhoff stress tensors yields the linear relation

$$S_{ij} = C_{ijkl}\left(E_{kl} - E_{kl}^{(th)}\right) \tag{8}$$

where $\underline{\underline{E}}^{(th)}$ denotes the strain tensor arising from the potential thermal effects. This tensor can be expressed as

$$\underline{\underline{E}}^{(th)} = T\,\underline{\underline{C}}^{(th)} \tag{9}$$

where $\underline{\underline{C}}^{(th)}$ is the thermal expansion tensor. Finally, the fourth order elasticity tensor $\underline{\underline{C}}$ satisfies the symmetry conditions

$$C_{ijkl} = C_{jikl} = C_{ijlk} = C_{klij} \tag{10}$$

and the positive definiteness property

$$A_{ij} \, C_{ijkl} \, A_{kl} \geq 0 \tag{11}$$

for any second order tensor $\underline{\underline{A}}$.

REDUCED ORDER MODELING
The previous section has provided the governing equations for the infinite dimensional problem of determining the stress and displacement fields everywhere in the structure considered. Following the discussion of the introduction, it is next desired to construct finite dimensional reduced order models of Eqs (1)-(9) that can be used for a nonparametric stochastic modeling of uncertainty. Before introducing the basis for the reduction, it is necessary to express the problem in its weak form.

To this end, denote by $\underline{v} = \underline{v}(\underline{X})$ a vector function of $\underline{X}$ that is sufficiently differentiable and such that $\underline{v} = \underline{0}$ on $\partial\Omega_0^u$. Then, the weak formulation of the geometric nonlinear elastodynamic problem of Eqs (3)-(5) is to find the displacement field $\underline{u}$ such that

$$\int_{\Omega_0} \rho_0 \, v_i \, \ddot{u}_i \, d\underline{X} + \int_{\Omega_0} \frac{\partial v_i}{\partial X_k} \left(F_{ij} \, S_{jk} \right) d\underline{X} = \int_{\Omega_0} \rho_0 \, v_i \, b_i^0 \, d\underline{X} + \int_{\partial\Omega_0^t} v_i \, t_i^0 \, ds \tag{12}$$

is satisfied for all v_i satisfying the above conditions.

A reduced order model of the nonlinear geometric problem can then be obtained by assuming the displacement field $\underline{u}$ in the form

$$u_i(\underline{X}, t) = \sum_{n=1}^{M} q_n(t) \, U_i^{(n)}(\underline{X}) \tag{13}$$

and applying Eq. (10) with $v_i = U_i^{(m)}$ for $m = 1, 2, ..., M$ where M is the order of the model, i.e. the number of basis functions $U_i^{(m)}$ in Eq. (11). After some algebraic manipulations, this process yields

$$M_{ij} \, \ddot{q}_j + D_{ij} \, \dot{q}_j + \left[K_{ij}^{(1)} - K_{ij}^{(th)} \right] q_j + K_{ijl}^{(2)} \, q_j \, q_l + K_{ijlp}^{(3)} \, q_j \, q_l \, q_p = F_i + F_i^{(th)} \tag{14}$$

where

$$M_{mn} = \int_{\Omega_0} \rho_0 \, U_i^{(m)} \, U_i^{(n)} d\underline{X} \tag{15}$$

$$K_{mn}^{(1)} = \int_{\Omega_0} \frac{\partial U_i^{(m)}}{\partial X_k} C_{iklp} \frac{\partial U_l^{(n)}}{\partial X_p} d\underline{X} \tag{16}$$

$$K_{mnp}^{(2)} = \frac{1}{2} \left[\hat{K}_{mnp}^{(2)} + \hat{K}_{pmn}^{(2)} + \hat{K}_{npm}^{(2)} \right] \tag{17}$$

$$\hat{K}_{mnp}^{(2)} = \int_{\Omega_0} \frac{\partial U_i^{(m)}}{\partial X_j} C_{ijkl} \frac{\partial U_r^{(n)}}{\partial X_k} \frac{\partial U_r^{(p)}}{\partial X_l} d\underline{X} \tag{18}$$

$$K^{(3)}_{msnp} = \frac{1}{2} \int_{\Omega_0} \frac{\partial U^{(m)}_i}{\partial X_j} \frac{\partial U^{(s)}_i}{\partial X_k} C_{jklw} \frac{\partial U^{(n)}_r}{\partial X_l} \frac{\partial U^{(p)}_r}{\partial X_w} d\underline{X} \tag{19}$$

$$K^{(th)}_{mn} = \int_{\Omega_0} \frac{\partial U^{(m)}_i}{\partial X_k} \frac{\partial U^{(n)}_i}{\partial X_j} C_{jklr} E^{(th)}_{lr} d\underline{X} \tag{20}$$

$$F_m = \int_{\Omega_0} \rho_0 U^{(m)}_i b^0_i d\underline{X} + \int_{\partial\Omega^t_0} U^{(m)}_i t^0_i ds \tag{21}$$

and, finally,

$$F^{(th)}_m = \int_{\Omega_0} \frac{\partial U^{(m)}_i}{\partial X_k} C_{iklr} E^{(th)}_{lr} d\underline{X} . \tag{22}$$

Following standard practice, a damping term $D_{ij} \dot{q}_j$ has been added in Eq. (14) to represent various dissipation mechanisms.

The matrices and tensors involved in Eq. (14) have a variety of properties that arise both from their definitions and the characteristics of the elasticity tensor $\underline{\underline{C}}$, see Eqs (10) and (11). In particular and as expected, it is readily shown that $\underline{M}$ and $\underline{K}^{(1)}$ are both symmetric and positive definite. Further, it is seen from Eqs (10) and (18) that $\hat{K}^{(2)}_{mnp} = \hat{K}^{(2)}_{mpn}$ which, coupled with the definition of $K^{(2)}_{mnp}$, Eq. (17), implies that $K^{(2)}_{mnp}$ is invariant under any permutation of its indices. Next, it is found from Eqs (10) and (19) that the fourth order tensor $\underline{\underline{K}}^{(3)}$ exhibits the same symmetry properties, i.e. Eq. (10), as $\underline{\underline{C}}$ and further that it is also positive definite.

In addition to the above properties, which involve each matrix separately, there is also one notable property that involves $\underline{K}^{(1)}$, $\hat{\underline{\underline{K}}}^{(2)}$, and $\underline{\underline{K}}^{(3)}$ together. To demonstrate it, consider the reshaping operating that transforms the MxMxM third order tensor $\hat{\underline{\underline{K}}}^{(2)}$ into a MxM^2 rectangular array $\tilde{\underline{\underline{K}}}^{(2)}$ and the MxMxMxM fourth order tensor $\underline{\underline{K}}^{(3)}$ into a M^2xM^2 square matrix $\tilde{\underline{\underline{K}}}^{(3)}$. These operations are achieved as follows:

$$\tilde{K}^{(2)}_{mJ} = \hat{K}^{(2)}_{mnp} \qquad \text{with} \qquad J=(n\text{-}1)M+p \tag{23}$$

and

$$\tilde{K}^{(3)}_{IJ} = K^{(3)}_{msnp} \qquad \text{with} \quad I=(m\text{-}1)M+s \quad \text{and} \quad J=(n\text{-}1)M+p. \tag{24}$$

Next, denote similarly

$$Z^{(J)}_{kl} = \frac{\partial U^{(n)}_r}{\partial X_k} \frac{\partial U^{(p)}_r}{\partial X_l} \tag{25}$$

and introduce the PxP symmetric matrix $\underline{\underline{K}}_B$ as

$$\underline{\underline{K}}_B = \begin{bmatrix} \underline{\underline{K}}^{(1)} & \underline{\underline{\tilde{K}}}^{(2)} \\ \underline{\underline{\tilde{K}}}^{(2)T} & 2\underline{\underline{\tilde{K}}}^{(3)} \end{bmatrix} \tag{26}$$

where $P = M + M^2$.

It is next desired to demonstrate that $\underline{\underline{K}}_B$ is positive definite. To this end, introduce first the P-component vector $\underline{W}$ partitioned as

$$\underline{W}^T = \begin{bmatrix} \underline{q}^T & \underline{V}^T \end{bmatrix} \tag{27}$$

where $\underline{q}$ and $\underline{V}$ have M and M^2 components, respectively. Next, note that

$$\underline{W}^T \underline{\underline{K}}_B \underline{W} = K_{mn}^{(1)} q_m q_n + 2\tilde{K}_{mJ}^{(2)} q_m V_J + 2\tilde{K}_{IJ}^{(3)} V_I V_J$$

$$= \int_{\Omega_0} \left\{ \left(q_m \frac{\partial U_i^{(m)}}{\partial X_k} \right) C_{iklp} \left(q_n \frac{\partial U_l^{(n)}}{\partial X_p} \right) + 2\left(q_m \frac{\partial U_i^{(m)}}{\partial X_j} \right) C_{ijkl} \left(V_J Z_{kl}^{(J)} \right) + \left(V_I Z_{jk}^{(I)} \right) C_{jklw} \left(V_J Z_{lw}^{(J)} \right) \right\} d\underline{X} \tag{28}$$

Renaming the dummy indices in the above equation and using the symmetries of Eq. (10), it is found that

$$\underline{W}^T \underline{\underline{K}}_B \underline{W} = \int_{\Omega_0} \left(q_m \frac{\partial U_i^{(m)}}{\partial X_j} + V_I Z_{ij}^{(I)} \right) C_{ijkl} \left(q_n \frac{\partial U_k^{(n)}}{\partial X_l} + V_J Z_{kl}^{(J)} \right) d\underline{X} \tag{29}$$

which is positive for all vectors $\underline{q}$ and $\underline{V}$ given Eq. (11). It is then concluded that the matrix $\underline{\underline{K}}_B$ is indeed positive definite. Note that this property also implies the positive definiteness of $\underline{\underline{K}}^{(1)}$ and $\underline{\underline{K}}^{(3)}$ which was stated earlier.

The availability of the displacement field in the form of Eq. (13) leads to the knowledge of all quantities of interest in both reference and deformed configurations. For example, combining Eqs (1), (2), (8), and (13) leads to the expression for any component of the second Piola-Kirchhoff stress tensor as

$$S_{ij} = \bar{S}_{ij} + \sum_m \hat{S}_{ij}^{(m)} q_m + \sum_{m,n} \tilde{S}_{ij}^{(m,n)} q_m q_n \tag{30}$$

where

$$\bar{S}_{ij} = -C_{ijkl} E_{kl}^{(th)} \tag{31}$$

$$\hat{S}_{ij}^{(m)} = C_{ijkl} \frac{\partial U_k^{(m)}}{\partial X_l} \tag{32}$$

and

$$\tilde{S}_{ij}^{(m,n)} = \frac{1}{2} C_{ijkl} \frac{\partial U_r^{(m)}}{\partial X_k} \frac{\partial U_r^{(n)}}{\partial X_l}. \tag{33}$$

ESTIMATION OF THE REDUCED ORDER MODEL PARAMETERS

Equations (15)-(22) provide direct expressions for all of the reduced order model parameters given the basis functions $U_i^{(m)}(\underline{X})$ and the geometrical and material properties of the structure, e.g. ρ_0, C_{ijkl},

Ω_0, etc., and thus, technically, complete the reduced order modeling strategy. In practice, however, it is likely that a finite element model of the structure is available and was relied upon to determine the basis functions $U_i^{(m)}(\underline{X})$. Then, the integration over Ω_0 should be split into integrals over the various elements forming the mesh and the appropriate interpolation functions should be used to evaluate the basis functions $U_i^{(m)}(\underline{X})$ and their derivatives. Although fairly straightforward, this effort appears quite cumbersome and may require a more detailed knowledge of the inner workings of the finite element package used than may be available, especially for commercially available codes. Accordingly, it would be very desirable to dispose of an indirect approach to determine the various stiffness and mass terms that is compatible with standard finite element packages. One such technique, referred to as the STEP method (STiffness Evaluation Procedure), was initially conceived in [7] and later modified in [8, 9].

The fundamental idea behind the STEP approach is to identify the stiffness parameters $K_{ij}^{(1)} - K_{ij}^{(th)}$, $K_{ijl}^{(2)}$, and $K_{ijlp}^{(3)}$ by successive static finite element computations in which the displacement field is prescribed to $\underline{u}(X)$ and the required surface tractions $\underline{t}^0$ are estimated under the prescribed temperature field. The STEP approach starts with the imposition of displacement fields that are proportional to a single basis function, i.e.,

$$\bar{u}_i^{(1)}(\underline{X}) = q_n^{(1)}\, U_i^{(n)}(\underline{X}); \; \bar{u}_i^{(2)}(\underline{X}) = q_n^{(2)}\, U_i^{(n)}(\underline{X}) \text{ and } \bar{u}_i^{(3)}(\underline{X}) = q_n^{(3)}\, U_i^{(n)}(\underline{X}) \qquad (34)$$

for each value of n in turn. In these conditions, $q_n^{(1)}, q_n^{(2)}$, and $q_n^{(3)}$ are three constants scaling factors differing from each other and such that the displacements induced ($\bar{u}_i^{(p)}$) are large enough to induce significant geometric nonlinear effects but small enough to stay within the convergence limits of the finite element code. Inserting the imposed displacement fields of Eq. (34) in Eq. (14) implies that

$$\left[K_{in}^{(1)} - K_{in}^{(th)}\right] q_n^{(1)} + K_{inn}^{(2)} \left(q_n^{(1)}\right)^2 + K_{innn}^{(3)} \left(q_n^{(1)}\right)^3 = F_i^{n(1)} + F_i^{(th)} \qquad (35)$$

$$\left[K_{in}^{(1)} - K_{in}^{(th)}\right] q_n^{(2)} + K_{inn}^{(2)} \left(q_n^{(2)}\right)^2 + K_{innn}^{(3)} \left(q_n^{(2)}\right)^3 = F_i^{n(2)} + F_i^{(th)} \qquad (36)$$

$$\left[K_{in}^{(1)} - K_{in}^{(th)}\right] q_n^{(3)} + K_{inn}^{(2)} \left(q_n^{(3)}\right)^2 + K_{innn}^{(3)} \left(q_n^{(3)}\right)^3 = F_i^{n(3)} + F_i^{(th)} \qquad (37)$$

where the force terms $F_i^{n(p)}$, p=1, 2, or 3, are computed by Eq. (21) from the traction $\underline{t}^0$ predicted in each case by the finite element code. If the thermal force $F_i^{(th)}$ is known, e.g. equal to zero by symmetry, Eqs (35)-(37) represent for each i and n a set of three linear equations in the unknown $K_{in}^{(1)} - K_{in}^{(th)}, K_{inn}^{(2)}$, and $K_{innn}^{(3)}$ which is readily solved. If the thermal force $F_i^{(th)}$ is unknown, its value must first be estimated by imposing a zero displacement field and proceeding as above from the tractions $\underline{t}^0$ required to maintain the equilibrium. Denoting the corresponding force term as $F_i^{n(0)}$, it is found that $F_i^{(th)} = -F_i^{n(0)}$.

The next stage of the STEP algorithm focuses on the determination of the parameters $K_{imn}^{(2)}$, $K_{immn}^{(3)}$, and $K_{imnn}^{(3)}$ (and their permutations of indices, see discussion on properties of $\underline{\underline{K}}^{(2)}$ and $\underline{\underline{K}}^{(3)}$) with $m \neq n$. This computation is again achieved by imposing displacement fields and determining the necessary tractions $\underline{t}^0$ and associated force terms F_i, Eq. (21). However, the procedure is slightly different from the one above in that involving the parameters $K_{imn}^{(2)}$, $K_{immn}^{(3)}$, and $K_{imnn}^{(3)}$ requires a displacement field that has components in both U_i^n and U_i^m, i.e.

$$\bar{u}_i^{(4)}(\underline{X}) = q_n^{(4)} \, U_i^{(n)}(\underline{X}) + q_m^{(4)} \, U_i^{(m)}(\underline{X}) \quad ; \quad \bar{u}_i^{(5)}(\underline{X}) = q_n^{(5)} \, U_i^{(n)}(\underline{X}) + q_m^{(5)} \, U_i^{(m)}(\underline{X})$$

and $$\bar{u}_i^{(6)}(\underline{X}) = q_n^{(6)} \, U_i^{(n)}(\underline{X}) + q_m^{(6)} \, U_i^{(m)}(\underline{X}). \tag{38}$$

Expressing the reduced order model governing equation, Eq. (14), for these 3 displacement fields and the associated force terms $F_i^{n(p)}$, $p = 4$, 5, and 6, yields a set of three equations for each i, m, and n which is readily solved to obtain the parameters $K_{imn}^{(2)}$, $K_{immn}^{(3)}$, and $K_{imnn}^{(3)}$. The choice of scaling factors $q_n^{(4)} = q_n^{(5)} = -q_n^{(6)}$ and $q_m^{(4)} = -q_m^{(5)} = -q_m^{(6)}$ does lead to some simplifications of the equations.

The last stage of the STEP algorithm is concerned with the evaluation of the coefficients $K_{imns}^{(3)}$ (and its permutations of indices) for m, n, and s all different. This effort is readily achieved from the above results using the final displacement field

$$\bar{u}_i^{(7)}(\underline{X}) = q_n^{(7)} \, U_i^{(n)}(\underline{X}) + q_m^{(7)} \, U_i^{(m)}(\underline{X}) + q_s^{(7)} \, U_i^{(s)}(\underline{X}) \tag{39}$$

and the associated force term $F_i^{(7)}$.

The series of finite element computations performed for the evaluation of the stiffness parameters can serve as well for the estimation of the coefficients $\bar{S}_{ij}(\underline{X})$, $\hat{S}_{ij}^{(m)}(\underline{X})$, and $\tilde{S}_{ij}^{(m,n)}(\underline{X})$ of the reduced order model for the stress S_{ij} at location $\underline{X}$ provided that the values of this stress are output during each run. The procedure is similar to the one conducted above and will not be repeated here.

It should however be noted that the stress is a second order polynomial of the generalized coordinates q_n as compared to the cubic nature of the nonlinear stiffness terms. Thus, many fewer computations would be necessary to estimate $\bar{S}_{ij}(\underline{X})$, $\hat{S}_{ij}^{(m)}(\underline{X})$, and $\tilde{S}_{ij}^{(m,n)}(\underline{X})$ than are actually performed. The redundant cases can then be used to assess the accuracy of the estimates of these stress coefficients and thus provide a first mean to quantify the robustness of the STEP algorithm. A second perspective on this robustness can be obtained from a check of the symmetries of the tensors $\underline{\underline{K}}^{(1)}$, $\underline{\underline{K}}^{(th)}$, $\underline{\underline{K}}^{(2)}$, and $\underline{\underline{K}}^{(3)}$ which were *not* used in the determination of their components. For example, the properties $K_{ij}^{(1)} = K_{ji}^{(1)}$ and $K_{ij}^{(th)} = K_{ji}^{(th)}$ were not relied upon in Eqs (35)-(37). Similarly, the symmetry $K_{ijk}^{(2)} = K_{kij}^{(2)}$ was not used in the computations while the property $K_{ijk}^{(2)} = K_{ikj}^{(2)}$ *was* assumed. A similar discussion also holds

with the elements of $\underline{\underline{K}}^{(3)}$. A final perspective on the robustness of the STEP identification can be derived from the expected linearity of the thermal stiffness tensor $\underline{\underline{K}}^{(th)}$ with respect to temperature, see Eqs (9) and (20). A detailed discussion of these issues in connection with a flat plate (see [8]) has shown that there exists a fairly broad range of the scaling factors $q_i^{(p)}$ over which the estimates of the stiffness coefficients are accurate and stable.

NONPARAMETRIC STOCHASTIC MODELING OF UNCERTAINTY
As discussed in the introduction, there are two particular types of uncertainty to be considered in structural dynamic models: data uncertainty and model uncertainty. The former is associated with variations of the material properties of the structure that arise from the manufacturing process and/or in service operation. At the contrary, model uncertainty recognizes that the computational model is a simplified representation of the physical structure. For example, components such as fasteners (rivets, bolts,...) and joints (lap joints, welds, ...) etc. are usually only approximately represented, i.e. *modeled*. A similar discussion holds with the geometry of the structure which differs slightly from the computational one, plates may be slightly warped, beams out of straight, etc. Thus, deviations in the behaviors of actual structures and their computational counterparts are expected and variable and form the model uncertainty.

The consideration of data uncertainty in the infinite dimensional problem of Eqs (1)-(9) is in principle quite straightforward, it can be achieved by letting the material properties ρ_0, $\underline{\underline{C}}$, $\underline{b}^0$, ... be random field. The inclusion of model uncertainty in the same framework is however very challenging. For example, the consideration of variations of geometry would require changing the computational model (i.e. the finite element mesh) for every realization of the geometry. The consideration of other model issues, as related to the approximate representation of joints, fasteners, etc. appears even more difficult if at all possible.

On the contrary, the consideration of uncertainty, from data or model, appears much more straightforward in the reduced order model, as it is characterized by a finite number of mass and stiffness coefficients which can be treated as random variables and are physically expected to be correlated. In addition to those coefficients, the reduced order model also involves the basis functions $U_i^{(n)}$ and it is worthwhile to ask whether that basis should be deterministic (i.e. related to the mean model) or random (e.g. based on the full computational model with some data uncertainty). The most significant advantage of using a random basis would be to obtain certain special properties of the random reduced order model, e.g. diagonal nature of some of the matrices involved. However, the inclusion of model uncertainty would likely destroy these special features. On the contrary, the use of a deterministic basis is computationally efficient as it needs to be determined only once and focuses the randomness of the reduced order model on its coefficients. On the basis of this discussion, deterministic basis functions will be adopted in the sequel but their choice must be such that the response of the *random* systems, not just the mean one, is well represented. Additional comments in this respect will be made in the Numerical Results section.

Data and model uncertainty will thus be included through randomizing the various mass and stiffness coefficients of Eq. (14), see Eqs (15)-(20). This apparently simple statement has far ranging implications as a complete characterization of this ensemble of random variables requires the specification of their joint probability density function, an information which is unlikely to be available in any practical

application. A first approach to resolve this difficulty is to allow only some of the coefficients to be random as was done in the ad-hoc strategies discussed in the Introduction. Clearly such an approach does not have the accuracy and generality required here. A second approach might be to specify the form of this distribution with unknown parameters to be estimated. Even with a single parameter per random coefficient to describe its variations, there would be a very large number of such parameters to estimate especially given the generally poor knowledge on the actual uncertainty in physical systems.

A third approach, which is the one adopted here, is to rely on a higher principle to *derive* the necessary joint probability density function. As discussed by Soize [3-6], the maximum entropy principle provides such a framework and leads to statistical distributions that place particular emphasis on "larger" deviations from the mean value, a desirable feature to assess the robustness of a design to uncertainty. The maximization of the entropy must however be achieved carefully to guarantee the physical meaningfulness of the ensemble of mass and stiffness coefficients simulated, especially in view of the emphasis on the tail of the distribution just stated. Physical meaningfulness of the mass and stiffness coefficients of the reduced order model of Eq. (14) implies here that these coefficients satisfy all properties that are expected from Eq. (14) for an *arbitrary* dynamic system, i.e.

(1) the stated symmetry properties of the tensors $\underline{\underline{\breve{M}}}$, $\underline{\underline{\breve{K}}}^{(1)}$, $\underline{\underline{\breve{K}}}^{(2)}$, $\underline{\underline{\breve{K}}}^{(3)}$, and $\underline{\underline{\breve{K}}}^{(th)}$

(2) the positive definiteness of the matrices $\underline{\underline{\breve{M}}}$ and $\underline{\underline{\breve{K}}}_B$

(3) the nonsingularity of the matrices $\underline{\underline{\breve{M}}}$ and $\underline{\underline{\breve{K}}}_B$ (if true for the mean model).

Note in the above conditions that $\underline{\underline{\breve{M}}}$ is the random mass matrix resulting from the consideration of uncertainty in contrast to the deterministic mass matrix $\underline{\underline{M}}$ of the mean model. A similar convention was also used above for $\underline{\underline{\breve{K}}}_B$, $\underline{\underline{\breve{K}}}^{(1)}$, $\underline{\underline{\breve{K}}}^{(2)}$, $\underline{\underline{\breve{K}}}^{(3)}$, and $\underline{\underline{\breve{K}}}^{(th)}$ and will be employed in the sequel to distinguish all random quantities.

The consideration of uncertainty in the reduced order model of Eq. (14) is then achieved by analyzing the response of the random system

$$\breve{M}_{ij}\,\ddot{\breve{q}}_j + \breve{D}_{ij}\,\dot{\breve{q}}_j + \left[\breve{K}_{ij}^{(1)} - \breve{K}_{ij}^{(th)}\right]\breve{q}_j + \breve{K}_{ijl}^{(2)}\,\breve{q}_j\,\breve{q}_l + \breve{K}_{ijlp}^{(3)}\,\breve{q}_j\,\breve{q}_l\,\breve{q}_p = \breve{F}_i + \breve{F}_i^{(th)} \tag{40}$$

in which a damping term, possibly stochastic, has been added. Note as well that the excitation F_i of Eq. (14) has been replaced by the random term $\breve{F}_i$ in Eq. (40). This randomization of the excitation reflects the possible random nature of the transport of the specified traction from the (random) deformed configuration back to the (deterministic) reference one.

In his original formulation of the nonparametric stochastic modeling approach, Soize [3,4] addressed the problem of determining the joint probability density function $p_{\underline{\underline{\breve{A}}}}(\underline{\underline{a}})$ of the elements $\breve{A}_{ij}$ of a random symmetric positive definite $\bar{n}x\bar{n}$ matrix $\underline{\underline{\breve{A}}}$ that maximizes the entropy

$$S = -\int_{\Omega} p_{\underline{\underline{\breve{A}}}}(\underline{\underline{a}})\ln p_{\underline{\underline{\breve{A}}}}(\underline{\underline{a}})d\underline{\underline{a}} \quad . \tag{41}$$

In this equation, Ω denotes the domain of support of $p_{\underline{\underline{\breve{A}}}}(\underline{\underline{a}})$ which should be such that any matrix $\underline{\underline{a}} \in \Omega$ is symmetric and positive definite. These conditions are equivalent to stating that $\underline{\underline{a}}$ admits a

Cholesky decomposition $\underline{\underline{a}} = \underline{\underline{L}}\,\underline{\underline{L}}^T$ so that

$$\Omega = \left\{ \underline{\underline{a}} = \underline{\underline{L}}\,\underline{\underline{L}}^T\,; L_{ij}\,, i,j = 1,...,\bar{n} : \left[L_{ij} \in (-\infty,+\infty), i > j\right] \cap \left[L_{ii} \in [0,+\infty)\right] \right\}. \tag{42}$$

The maximization of S, Eq. (41), must be achieved under the following constraints

$$\int_\Omega p_{\underline{\underline{\breve{A}}}}(\underline{\underline{a}})\,d\underline{\underline{a}} = 1 \tag{43}$$

$$E\left[\underline{\underline{\breve{A}}}\right] = \int_\Omega \underline{\underline{a}}\; p_{\underline{\underline{\breve{A}}}}(\underline{\underline{a}})\,d\underline{\underline{a}} = \underline{\underline{A}} \tag{44}$$

and

$$\int_\Omega \ln\left[\det(\underline{\underline{a}})\right] p_{\underline{\underline{\breve{A}}}}(\underline{\underline{a}})\,d\underline{\underline{a}} = \nu \;\text{ finite} \tag{45}$$

where $E[.]$ denotes the operation of mathematical expectation and $\det(\underline{\underline{W}})$ is the determinant of an arbitrary matrix $\underline{\underline{W}}$. The first two of the above constraints correspond to the normalization of the total probability to 1 (Eq. (43)) and the specification of the mean matrix (Eq. (44)). The third one, Eq. (45), implies the existence of the mean squared Frobenius norm of the inverse matrix $\underline{\underline{\breve{A}}}^{-1}$ (see [3,4] for discussion) and thus guarantees the nonsingularity of $\underline{\underline{\breve{A}}}$ for mean square convergence.

The determination of the probability density function maximizing Eq. (41) while satisfying the constraints of Eqs (43)-(45) was accomplished in [3,4] by calculus of variations with Lagrange multipliers. The resulting stochastic description of $\underline{\underline{\breve{A}}}$ is most easily stated in terms of the random lower triangular matrix $\underline{\underline{\breve{H}}}$ such that

$$\underline{\underline{\breve{A}}} = \underline{\underline{\bar{L}}}\,\underline{\underline{\breve{H}}}\,\underline{\underline{\breve{H}}}^T\,\underline{\underline{\bar{L}}}^T \tag{46}$$

where $\underline{\underline{\bar{L}}}$ is any decomposition, e.g. Cholesky, of $\underline{\underline{A}}$ satisfying $\underline{\underline{A}} = \underline{\underline{\bar{L}}}\,\underline{\underline{\bar{L}}}^T$. Specifically, it was found [3,4] that

$$p_{\underline{\underline{\breve{H}}}}(\underline{\underline{h}}) = \prod_{i=1}^{\bar{n}} \left\{ \bar{C}_i\, h_{ii}^{p(i)} \exp\left[-\mu_{ii}\, h_{ii}^2\right] \right\} \times \prod_{i=1}^{\bar{n}} \prod_{l=1}^{i-1} \left\{ \bar{C}_{il}\, \exp\left[-\mu_{ii}\, h_{il}^2\right] \right\} \tag{47}$$

where $\bar{C}_i$, $i=1,...,\bar{n}$, and $\bar{C}_{il}$, $i=1,...,\bar{n}$; $l=1,...,i$-1, are appropriate normalization constants and

$$p(i) = \bar{n} - i + 2\lambda - 1 \tag{48}$$

$$\mu_{ii} = \frac{\bar{n} + 2\lambda - 1}{2}\;. \tag{49}$$

It is concluded from Eq. (47) that:

(i) the elements $\breve{H}_{il}$, $i>l$, are all independent of each other and independent of the elements $\breve{H}_{ii}$. Further, they are normally distributed with mean 0 and standard deviation $\sigma_{il} = 1/\sqrt{2\mu_{ii}}$.

(ii) the elements $\breve{H}_{ii}$ are all independent of each other. Further, they are distributed according to

$$p_{\breve{H}_{ii}}(h_{ii}) = \overline{C}_i \, h_{ii}^{p(i)} \exp\left[-\mu_{ii} \, h_{ii}^2\right], \ h_{ii} \geq 0 \tag{50}$$

where

$$\overline{C}_i = \frac{2\mu_{ii}^{[p(i)+1]/2}}{\Gamma((p(i)+1)/2)} \tag{51}$$

and $\Gamma(.)$ denotes the Gamma function.

The generation of samples of $\breve{H}_{ii}$ is simplified by considering the variable $\breve{Y}_{ii} = \mu_{ii} \, \breve{H}_{ii}^2$. Proceeding with the change of variables, it is found that the probability density function of $\breve{Y}_{ii}$ is

$$p_{\breve{Y}_{ii}}(y_{ii}) = \frac{y_{ii}^{(p(i)-1)/2}}{\Gamma[(p(i)+1)/2]} \exp[-y_{ii}], \ y_{ii} \geq 0 . \tag{52}$$

Accordingly, it is found that $\breve{Y}_{ii}$ is a Gamma distributed random variable for which efficient simulation algorithms exist, e.g. see [13]. Once a sample of $\breve{Y}_{ii}$ has been simulated according to the Gamma distribution, the corresponding value of $\breve{H}_{ii}$ is found as

$$\breve{H}_{ii} = \sqrt{\frac{\breve{Y}_{ii}}{\mu_{ii}}} \tag{53}$$

where μ_{ii} is given by Eq. (49).

The parameter λ which appears in Eq. (48) and (49) is in fact the Lagrange multiplier associated with the constraint of Eq. (45) and could be evaluated from this condition. However, since Eq. (45) was enforced to ensure an appropriately flat zero of $p_{\breve{A}}(a)$ near its singular boundary (i.e. an appropriately flat zero of $p_{\breve{H}_{ii}}(h_{ii})$ at $h_{ii} = 0$), it is more appropriate to use the parameter λ to control the variations of the random matrices $\underline{\breve{A}}$ from their mean value $\underline{A}$, as will be clarified in the Numerical Results section.

Equations (46)-(53) form the core methodology for the simulation of the random mass, damping, and stiffness coefficients of Eq. (41) as follows.

For the random mass matrix $\underline{\breve{M}}$:
A Cholesky decomposition of the mass matrix of the mean model $\underline{M}$ is first performed as

$$\underline{M} = \underline{\overline{L}}_M \, \underline{\overline{L}}_M^T . \tag{54}$$

Next, a value $\lambda = \lambda_M$ is specified and an ensemble of $\overline{n} \mathrm{x} \overline{n}$ lower triangular matrices $\underline{\breve{H}}_M$, with $\overline{n} = M$, are generated according to Eq. (46)-(53). For each realization of $\underline{\breve{H}}_M$, the corresponding sample of the mass matrix $\underline{\breve{M}}$ is generated as

$$\underline{\breve{M}} = \underline{\overline{L}}_M \, \underline{\breve{H}}_M \, \underline{\breve{H}}_M^T \, \underline{\overline{L}}_M^T . \tag{55}$$

For the random damping matrix $\underline{\breve{D}}$:

A Cholesky decomposition of the damping matrix of the mean model $\underline{\underline{D}}$ is first performed as

$$\underline{\underline{D}} = \overline{\underline{\underline{L}}}_D \, \overline{\underline{\underline{L}}}_D^T. \tag{56}$$

Next, a value $\lambda = \lambda_D$ is specified and an ensemble of $\overline{n} \times \overline{n}$ lower triangular matrices $\underline{\underline{\breve{H}}}_D$, with $\overline{n} = M$, are generated according to Eq. (46)-(53). For each realization of $\underline{\underline{\breve{H}}}_D$, the corresponding sample of the damping matrix $\underline{\underline{\breve{D}}}$ is generated as

$$\underline{\underline{\breve{D}}} = \overline{\underline{\underline{L}}}_D \, \underline{\underline{\breve{H}}}_D \underline{\underline{\breve{H}}}_D^T \, \overline{\underline{\underline{L}}}_D^T. \tag{57}$$

For the random stiffness tensors $\underline{\underline{\breve{K}}}^{(1)}$, $\underline{\underline{\breve{K}}}^{(2)}$, and $\underline{\underline{\breve{K}}}^{(3)}$:

A Cholesky decomposition of the matrix $\underline{\underline{K}}_B$ of the mean model is first performed as

$$\underline{\underline{K}}_B = \overline{\underline{\underline{L}}}_K \, \overline{\underline{\underline{L}}}_K^T. \tag{58}$$

Next, a value $\lambda = \lambda_K$ is specified and an ensemble of $\overline{n} \times \overline{n}$ lower triangular matrices $\underline{\underline{\breve{H}}}_K$, with $\overline{n} = M + M^2$, are generated according to Eq. (46)-(53). For each realization of $\underline{\underline{\breve{H}}}_K$, the corresponding sample of the matrix $\underline{\underline{\breve{K}}}_B$ is generated as

$$\underline{\underline{\breve{K}}}_B = \overline{\underline{\underline{L}}}_K \, \underline{\underline{\breve{H}}}_K \underline{\underline{\breve{H}}}_K^T \, \overline{\underline{\underline{L}}}_K^T. \tag{59}$$

The partitioning of the random matrix $\underline{\underline{\breve{K}}}_B$ is consistent with the one of its mean value, i.e. Eq. (26), and thus permits to extract the corresponding random matrices $\underline{\underline{\breve{K}}}^{(1)}$, $\underline{\underline{\breve{\widetilde{K}}}}^{(2)}$, and $\underline{\underline{\breve{\widetilde{K}}}}^{(3)}$. No further manipulation is needed in connection with the linear stiffness matrix $\underline{\underline{\breve{K}}}^{(1)}$ but $\underline{\underline{\breve{\widetilde{K}}}}^{(2)}$ and $\underline{\underline{\breve{\widetilde{K}}}}^{(3)}$ must next be reshaped into random third and fourth order tensors $\underline{\underline{\breve{\widetilde{K}}}}^{(2NS)}$ and $\underline{\underline{\breve{K}}}^{(3NS)}$ as in Eq. (23) and (24) for $\underline{\underline{\hat{K}}}^{(2)}$ and $\underline{K}^{(3)}$ from $\underline{\underline{\widetilde{K}}}^{(2)}$ and $\underline{\underline{\widetilde{K}}}^{(3)}$. Note that the additional superscript NS indicates that these matrices do not exhibit the appropriate symmetries, for example $\breve{\widetilde{K}}_{mnp}^{(2NS)}$ is in general not equal to $\breve{\widetilde{K}}_{mpn}^{(2NS)}$. This issue is easily resolved and tensors $\underline{\underline{\breve{\widetilde{K}}}}^{(2)}$ and $\underline{\underline{\breve{K}}}^{(3)}$ with the appropriate symmetries are then generated as

$$\breve{\widetilde{K}}_{mnp}^{(2)} = \frac{1}{2}\left(\breve{\widetilde{K}}_{mnp}^{(2NS)} + \breve{\widetilde{K}}_{mpn}^{(2NS)} \right) \tag{60}$$

and

$$\breve{K}_{msnp}^{(3)} = \frac{1}{4}\left(\breve{K}_{msnp}^{(3NS)} + \breve{K}_{smnp}^{(3NS)} + \breve{K}_{mspn}^{(3NS)} + \breve{K}_{smpn}^{(3NS)} \right) \tag{61}$$

since the property $\breve{K}_{msnp}^{(3NS)} = \breve{K}_{npms}^{(3NS)}$ already exists as a result of the symmetry of $\underline{\underline{\breve{K}}}_B$, see Eq. (59) and (26).

It remains finally to obtain the realization of the third order tensor $\breve{\underline{\underline{K}}}^{(2)}$ from $\breve{\hat{\underline{\underline{K}}}}^{(2)}$. This is achieved as in Eq. (17), i.e.

$$\breve{K}_{mnp}^{(2)} = \frac{1}{2}\left(\breve{\hat{K}}_{mnp}^{(2)} + \breve{\hat{K}}_{pmn}^{(2)} + \breve{\hat{K}}_{npm}^{(2)} \right). \tag{62}$$

For the random thermal stiffness matrix $\breve{\underline{\underline{K}}}^{(th)}$:

The STEP algorithm does not lead directly to the thermal stiffness matrix $\breve{\underline{\underline{K}}}^{(th)}$, rather it produces the elements of $\breve{\underline{\underline{K}}}^{(1)}$ - $\breve{\underline{\underline{K}}}^{(th)}$. Nevertheless, it is possible to separate the two terms by noticing that $\breve{\underline{\underline{K}}}^{(th)}$ is a linear function of the temperature field while $\breve{\underline{\underline{K}}}^{(1)}$ is independent of it (both neglecting variations of the elasticity tensor $\underline{\underline{C}}$ with temperature). Thus, the application of the STEP algorithm for 2 temperatures fields proportional to each other permits the separate identification of $\breve{\underline{\underline{K}}}^{(1)}$ and $\breve{\underline{\underline{K}}}^{(th)}$.

The tensors $\breve{\underline{\underline{K}}}^{(1)}$, $\breve{\underline{\underline{K}}}^{(2)}$, and $\breve{\underline{\underline{K}}}^{(3)}$ involve solely the elasticity tensor $\underline{\underline{C}}$ of components C_{ijkl} while the thermal stiffness matrix $\breve{\underline{\underline{K}}}^{(th)}$ is also a function of the thermal expansion matrix $\underline{\underline{C}}^{(th)}$. This observation motivates here the consideration of $\breve{\underline{\underline{K}}}^{(th)}$ as statistically independent of $\breve{\underline{\underline{K}}}^{(1)}$, $\breve{\underline{\underline{K}}}^{(2)}$, and $\breve{\underline{\underline{K}}}^{(3)}$.

Note next that the thermal stiffness matrix of an arbitrary structure is not guaranteed from Eq. (20) to be positive definite. In some cases, such a property does hold, e.g. for an isotropic linearly elastic material exhibiting positive thermal expansion coefficients and with T larger than the reference temperature T_0 at which the structure is undeformed in the absence of external loads. Accordingly, it is desired here to separate the simulation of $\breve{\underline{\underline{K}}}^{(th)}$ into two separate cases, i.e. with and without the requirement that $\breve{\underline{\underline{K}}}^{(th)}$ is positive definite.

When $\breve{\underline{\underline{K}}}^{(th)}$ is required to be positive definite, and thus with $\underline{\underline{K}}^{(th)}$ satisfying this property, the simulation procedure closely parallel that of the mass and damping matrices. That is, a Cholesky decomposition of $\underline{\underline{K}}^{(th)}$ is first performed as

$$\underline{\underline{K}}^{(th)} = \overline{\underline{\underline{L}}}_{Kth}\, \overline{\underline{\underline{L}}}_{Kth}^{T}. \tag{63}$$

Next, a value $\lambda = \lambda_{Kth}$ is specified and an ensemble of $\bar{n} \times \bar{n}$ lower triangular matrices $\breve{\underline{\underline{H}}}_{Kth}$, with $\bar{n} = M$, are generated according to Eq. (46)-(53). For each realization of $\breve{\underline{\underline{H}}}_{Kth}$, the corresponding sample of the thermal stiffness matrix $\breve{\underline{\underline{K}}}^{(th)}$ is generated as

$$\breve{\underline{\underline{K}}}^{(th)} = \overline{\underline{\underline{L}}}_{Kth}\, \breve{\underline{\underline{H}}}_{Kth}\, \breve{\underline{\underline{H}}}_{Kth}^{T}\, \overline{\underline{\underline{L}}}_{Kth}^{T}. \tag{64}$$

When $\breve{\underline{\underline{K}}}^{(th)}$ is not required to be positive definite, the modified approach devised in [5] for rectangular arrays can be employed instead. In this approach, the mean model stiffness $\underline{\underline{K}}^{(th)}$ is first expressed in its right polar decomposition, i.e.

$$\underline{\underline{K}}^{(th)} = \underline{\underline{U}}^{(th)} \underline{\underline{T}}^{(th)} \tag{65}$$

where $\underline{\underline{T}}^{(th)}$ is the symmetric positive definite matrix satisfying

$$\left[\underline{\underline{T}}^{(th)}\right]^2 = \left[\underline{\underline{K}}^{(th)}\right]^2, \tag{66}$$

i.e. $\underline{\underline{T}}^{(th)}$ has the same eigenvectors as $\underline{\underline{K}}^{(th)}$ and its eigenvalues are the absolute values of the corresponding eigenvalues of $\underline{\underline{K}}^{(th)}$. Then,

$$\underline{\underline{U}}^{(th)} = \underline{\underline{K}}^{(th)} \left(\underline{\underline{T}}^{(th)}\right)^{-1} \tag{67}$$

so that $\underline{\underline{U}}^{(th)}$ also has the same eigenvectors as $\underline{\underline{K}}^{(th)}$ and its eigenvalues are the signum of the corresponding eigenvalues of $\underline{\underline{K}}^{(th)}$.

The generation of samples of the random matrix $\breve{\underline{\underline{T}}}^{(th)}$ is next achieved as in Eq. (63) and (64) for $\breve{\underline{\underline{K}}}^{(th)}$ when it is positive definite with the same values of $\bar{n}$ and λ. Finally, the corresponding random matrix $\breve{\underline{\underline{K}}}^{(th)}$ is obtained from the right polar decomposition as

$$\breve{\underline{\underline{K}}}^{(th)} = \underline{\underline{U}}^{(th)} \breve{\underline{\underline{T}}}^{(th)}. \tag{68}$$

In fact, the above procedure does generalize Eqs (63) and (64) as it reduces to these equations when $\underline{\underline{K}}^{(th)}$ is positive definite because then $\underline{\underline{T}}^{(th)} = \underline{\underline{K}}^{(th)}$ and $\underline{\underline{U}}^{(th)}$ is the identity matrix.

NUMERICAL RESULTS

To demonstrate the above concepts, a beam of dimensions 0.2286m long, 0.0127m wide, and 7.75 10^{-4}m was discretized by finite element (with MSC NASTRAN) into 40 CBEAM elements of equal lengths (some punctual computations were repeated with a 160 element model which confirmed the adequacy of the 40 element model). The two ends of the beam were assumed to be fully clamped. This model thus included 234 degrees-of-freedom. The beam material was high-carbon steel with a Young's modulus of 205,000 MPa, a shear modulus of 80,000 MPa, and a mass density of 7,875 kg/m^3. The damping in the mean system was assumed to be classical with a damping ratio of 2% on all modes.

The beam was assumed to be excited by a single, deterministic, concentrated force acting on its middle in the direction perpendicular to the beam axis, see Fig. 1 for a representative time history of the force and Fig. 2 for its frequency content, i.e. flat in the range [-2000, +2000] Hz.

The time marching of the response of the reduced order models (mean and random) was achieved with an unconditionally stable Newmark-β algorithm (e.g. see [14]) in which the nonlinear algebraic equations were solved by a fixed point algorithm. The time step for the most of the computations was set at $\Delta t = 5\,10^{-5}$s and the computations were carried out for $n_{tot} = 15000$ time steps. No convergence

problem with the fixed point algorithm was encountered with the above time step.

The basis for the reduced order modeling effort included the first n_t transverse linear modes and n_i in-plane linear modes exhibiting the natural frequencies shown in Table 1. The selection of the appropriate values of n_t and n_i was performed in each case by monitoring the convergence of the total modal signal energy of the mean model

$$E(n_t, n_i) = \sum_{n=1}^{n_{tot}} \sum_{i=1}^{M} q_i^2(n \, \Delta t) \tag{69}$$

where $M = n_t + n_i$ is the order of the reduced order model. In general, it was found that the selection $n_t = 10$ and $n_i = 12$ led to convergence. For the cases in which these parameters were changed, their values will be stated explicitly. It should be noted that the mean system is symmetric with respect to the location of the force and thus the second, fourth, and sixth transverse modes, which are antisymmetric, will not appear in the mean model response. However, the introduction of randomness in the beam reduced order model will in general break the symmetry and induce contributions of the response on these antisymmetric transverse modes. The same observation holds in regards to the in-plane modes.

	1	2	3	4	5	6	7	8
Transverse	79	218	427	706	1055	1473	1961	2518
In-Plane	11168	22353	33573	44844	56184	67611	79143	90795
	9	10	11	12	13	14	15	16
Transverse	3144	3841	4606	5441	6345	7319	8363	9477
In-Plane	102588	114537	126662	138975				

Table 1. Natural frequencies (Hz) of the first transverse (weak bending)
and in-plane modes, mean model from NASTRAN.

The direction of the force induced transverse motions in the weak bending direction ("z") with much smaller motions along the beam axis ("x") taking place by nonlinear interaction. The magnitude of these displacements satisfied the assumptions of the von Karman strain definition, which was adopted by NASTRAN, i.e.

$$\varepsilon_x = \frac{\partial u_1}{\partial x} + \frac{1}{2}\left(\frac{\partial u_3}{\partial x}\right)^2 \qquad \varepsilon_y = \frac{\partial u_2}{\partial y} + \frac{1}{2}\left(\frac{\partial u_3}{\partial y}\right)^2 \qquad \varepsilon_z = \frac{\partial w}{\partial z} = 0 \tag{70}$$

$$\gamma_{xy} = \frac{1}{2}\left[\frac{\partial u_1}{\partial y} + \frac{\partial u_2}{\partial x} + \left(\frac{\partial u_3}{\partial x}\right)\left(\frac{\partial u_3}{\partial y}\right)\right] \quad \gamma_{xz} = \frac{1}{2}\left[\frac{\partial u_1}{\partial z} + \frac{\partial u_3}{\partial x}\right] \quad \gamma_{yz} = \frac{1}{2}\left[\frac{\partial u_2}{\partial z} + \frac{\partial u_3}{\partial y}\right]$$

Note that the above expressions result from Eq. (2) by ignoring the second order terms in u_1 and u_2. In fact, the displacement u_2 is identically zero for this problem. The use of the von Karman strain definition by NASTRAN led to a peculiarity of the matrix $\underline{\underline{K}}_B$. Specifically, the absence of second order terms in u_1 in the displacement-strain relation can be shown to imply the vanishing of all terms $K_{mnp}^{(2)}$ and $K_{msnp}^{(3)}$ in which two or more indices m, n, p, and s refer to in-plane modes. This property leads theoretically to a matrix $\underline{\underline{K}}_B$ exhibiting a significant number of zero eigenvalues and computationally (given the finite accuracy of the STEP algorithm) to the same number of small generally both positive and negative eigenvalues. Clearly, the negative eigenvalues are unphysical (see

Eq. (29)) and must be removed before the consideration of uncertainty takes place. In doing so, it is necessary to demonstrate that these computationally negative values do not have an effect on the response. This check was accomplished on the mean model by computing the response with the identified $\underline{\underline{K}}_B$ matrix (exhibiting small negative eigenvalues) and the singular value decomposition of $\underline{\underline{K}}_B$ in which only the positive eigenvalues were retained. In all cases considered, the match of the two transverse responses at the middle point were in a visually perfect agreement over both entire time history and frequency range.

The elimination of the negative eigenvalues of $\underline{\underline{K}}_B$ by singular value decomposition led to the modified matrix $\underline{\underline{K}}'_B$ defined as

$$\underline{\underline{K}}'_B = \underline{\underline{\Phi}}\,\underline{\underline{\Lambda}}\,\underline{\underline{\Phi}}^T \tag{71}$$

where $\underline{\underline{\Phi}}$ denotes the matrix whose $n_r < M + M^2$ columns are the eigenvectors of $\underline{\underline{K}}_B$ corresponding to its positive eigenvectors. Further, $\underline{\underline{\Lambda}}$ is the diagonal matrix containing the n_r positive eigenvalues of $\underline{\underline{K}}_B$. Then, following Soize [5], the simulation of random matrices $\underline{\underline{\breve{K}}}_B$ is achieved by first generating an ensemble of $\bar{n}\mathrm{x}\bar{n}$ lower triangular matrices $\underline{\underline{\breve{H}}}_{Kr}$, with $\bar{n} = n_r$ and $\lambda = \lambda_{Kr}$ according to Eq. (46)-(53). Finally, the corresponding random matrices $\underline{\underline{\breve{K}}}_B$ are obtained as

$$\underline{\underline{\breve{K}}}_B = \left(\underline{\underline{\Phi}}\,\underline{\underline{\Lambda}}^{1/2}\right)\underline{\underline{\breve{H}}}_{Kr}\,\underline{\underline{\breve{H}}}_{Kr}^T\left(\underline{\underline{\Phi}}\,\underline{\underline{\Lambda}}^{1/2}\right)^T . \tag{72}$$

To enable a physical comparison between different cases, the various parameters λ should be selected to achieve the same physical measure of variation of the reduced order model. In the present investigation, the measure of variation specified related to the first natural frequency. More specifically, a 4% mean square variation of the first natural frequency of the random system (Ω_1) around its corresponding value for the mean model (ω_1) was enforced. That is,

$$E\left[(\Omega_1 - \omega_1)^2\right] = (0.04\,\omega_1)^2 . \tag{73}$$

The evaluation of the parameter λ from this condition was achieved in a trial and error strategy: for a value of λ, an ensemble of reduced order models were generated and the corresponding population of the first natural frequency of the random linear system were determined. An estimate of $E\left[(\Omega_1 - \omega_1)^2\right]$ was then obtained and the process was repeated until Eq. (73) was satisfied.

Once the appropriate value of λ has been determined, the generation of samples of the mass and stiffness coefficients of the random reduced order model can be achieved and the corresponding realizations of the response time histories $\underline{\breve{q}}$ can be obtained by numerical integration of Eq. (40). But how many such samples should be generated? This issue was resolved here my monitoring, for each case separately, the convergence of the estimate of the mean modal signal energy

$$\frac{1}{n_{sam}}\sum_{i=1}^{n_{sam}}\sum_{n=1}^{n_{tot}}\underline{\breve{q}}^{(i)T}(n\,\Delta t)\,\underline{\breve{q}}^{(i)}(n\,\Delta t) \rightarrow E\left[\underline{\breve{q}}^T\,\underline{\breve{q}}\right] \tag{74}$$

where $\underline{\breve{q}}^{(i)}(n\,\Delta t)$ denotes the vector of the $n_t + n_i$ generalized coordinates of sample i at the nth time step.

A first goal of the present numerical efforts was to assess the effects of geometric nonlinearity on the response of the uncertain beams. To this end, three different cases were considered with uncertainty on the stiffness terms and in the absence of temperature. First, a linear computation was carried out by ignoring the quadratic and cubic terms in Eq. (40) and determining the response to the excitation of Figs 1 and 2. Second, a fully nonlinear computation was carried out with the same excitation. Finally, this last set of computations was repeated at a higher excitation level.

Shown in Figs 3 and 4 is the displacement of the mid point of the beam predicted from the linear mean model both in time (Fig. 3) and in frequency (Fig. 4) with 12 in-plane modes and 10 transverse. The sharp drop in energy right at the cut-off frequency (2000 Hz) and the sharp resonance peaks are distinctive of the linear system. A convergence study of the mean modal signal energy of the random linear system, see Fig. 5, demonstrated that 600 samples were sufficient for convergence. Then, various statistics of the response could be obtained. Of particular interest here was the physical deflection of the center of the beam, more specifically its frequency content. Shown in Fig. 6 are the mean, 5th, and 95th percentiles of the spectrum of the random response of the middle of the beam. These curves were obtained by determining at each frequency the mean, 5th, and 95th percentiles of the 600 spectrum values. Also presented on Fig. 6 is the response of the mean model (dashed lines). Note in this figure that the 5th-95th percentile band increases with increasing frequency and is broader near the resonances and antiresonances of the mean model. Further, the response of the mean model is significantly lower than the 5th percentile near/at the antiresonances but very close to the 95th percentile value in the neighborhood of the mean model resonant frequencies.

A similar analysis was next repeated for the *nonlinear* reduced order model subjected to the same excitation. The transverse displacement at the center of the beam obtained from the mean model is again shown both as function of time and frequency in Figs 7 and 8 for 12 in-plane modes and 10 transverse. Note the significant reduction in the peak response (by approximately 40%) as compared to the response of the linear system and that the peak displacement at the middle of the beam is of the order of twice the beam thickness. Important differences also occur in the frequency domain, more specifically broader and more numerous peaks as well as the disappearance of the sharp drop off at 2000Hz. A sample size of 600 realizations was again found well sufficient for convergence and led to the spectrum plot of Fig. 9. The observations drawn in connection with the linear system spectrum can be repeated here, i.e. the 5th-95th percentile band is largest at/near the peaks and valleys of the spectrum of the mean model thus forming complex shapes that may rapidly widen or narrow down. Since the location of the peaks of the response is a function of the response level of the system, it would be expected that the 5th-95th percentile band would shift to the right as the amplitude of the motions is increased. This expectation is confirmed on Fig. 10 which repeats the data of Fig. 9 as well as the 5th-95th band obtained with an excitation 2.25 times the one shown in Figs 1 and 2 which leads to a peak transverse displacement of approximately 3.5 thicknesses at the beam middle for the mean model (computations carried out with 12 transverse modes and 12 in-plane). Note as well the distortion of the uncertainty band as it shift to higher frequencies.

The coefficients $\overline{S}_{ij}$, $\hat{S}_{ij}^{(m)}$, and $\widetilde{S}_{ij}^{(m,n)}$ corresponding to the stress σ_x at the middle of the beam were also obtained by the STEP algorithm and enabled the analysis of the effects of uncertainty on this stress. Shown in Fig. 11 is the comparison of the 5th-95th percentile bands at the two nonlinear response levels of Fig. 10. The discussion carried out in comparison with this figure holds here as well, the band is distorted as it moves to the right due to higher response level. A comparison of the uncertainty bands of

the displacement and stress (Figs 10 and 11) indicate that the latter one is much more complex than the former one due to the large number of peaks of the spectrum, which itself results from the quadratic transformation of Eq. (30).

Uncertainty in the natural frequencies may originate from either the stiffnesses and/or the masses. In this light, it was desired to compare the uncertainty band associated with the 4% mean square variation of the natural frequencies assuming that it originates from stiffnesses alone (as done above) or masses alone. This comparison, shown in Fig. 12, demonstrate that the two 5th-95th percentile bands are very close together with the one associated with mass uncertainty typically slightly broader than its stiffness counterpart. This observation may be justified by considering a uniform relative change of all stiffnesses by a value α. Such a change may be reflected as a uniform change by $1/\alpha$ of all stiffnesses, linear and nonlinear. With α a random variable, this observation would suggest that the randomness in mass would be similar to a randomness in the stiffnesses in which there exists a strong positive correlation between the various linear and nonlinear terms, i.e. increases/decreases in the linear stiffness terms being matched by increases/decreases of the nonlinear terms. Such a positive correlation does imply a lower 5th percentile of the response and a higher 95th percentile, i.e. a broader band, as compared to the case in which linear and nonlinear stiffnesses do not exhibit a significant correlation as tends to be the case in the uncertain stiffness computations. Similar observations can be drawn from the uncertainty bands in the stress spectrum (not shown here for brevity).

The above computations were all carried out in the absence of any thermal effects. Temperature however is known to have significant effects on the dynamics of very slender beams as the one considered here as it may induce buckling. In fact, the buckling temperature of the beam considered here is only 1.56°C. To assess the joint effects of uncertainty and temperature, two set of computations were carried out. The first reproduced the analysis of Figs 7-9 but with a uniform temperature equal to 1.25°C or 80% of the buckling temperature and uncertainty only in the "structural" stiffness tensors $\underline{\underline{K}}^{(1)}$, $\underline{\underline{K}}^{(2)}$, and $\underline{\underline{K}}^{(3)}$ (16 transverse modes and 12 in-plane were used). In the second set of computations, uncertainty was introduced only on the thermal stiffness matrix $\underline{\underline{K}}^{(th)}$ with a value λ_{th} such that the mean square deviations of the first natural frequency of the heated beams from their mean model value would be the same in both computations. The corresponding displacement spectra mean and percentiles are shown in Fig. 13 for the uncertainty in structural stiffness and in Fig. 14 for the uncertainty in the thermal stiffness matrix. A comparison of these two figures demonstrates that the behavior of the two random systems near the first peak is very similar owing to the equality of the mean square variations of the first natural frequencies. However, completely different behaviors take place at higher frequencies. Specifically, the uncertainty in the structural stiffness affects the entire frequency range with increasing uncertainty bands as frequency increases as already observed in Figs 9-11. On the contrary, the effects of the uncertainty of the thermal stiffness matrix appear to be decreasing as the frequency increases. This observation is directly related to the relatively small value of the largest eigenvalue of $\underline{\underline{K}}^{(th)}$. Thus, the application of temperature, and consequently the uncertainty on $\underline{\underline{K}}^{(th)}$, affects strongly the response of the beam in the low frequency range but has very little effect on higher modes as seen in Figs 13 and 14.

The above discussions have all been relevant to a broad band excitation, i.e. similar to Figs 1 and 2 and it was wondered whether similar results would also be seen for a narrowband excitation, i.e. in the range [1000, 1500] Hz see Figs 15 and 16. Given the previous observations, only the effects of uncertainty on

the stiffness tensors $\underline{\underline{K}}^{(1)}$, $\underline{\underline{K}}^{(2)}$, and $\underline{\underline{K}}^{(3)}$ were considered and no thermal effect was considered. The computations were carried out with 16 transverse modes and 12 in plane modes at a time step of $\Delta t = 2.5\,10^{-5}$ s and the computations were carried out for $n_{tot} = 30000$ time steps. Shown in Figs 17 and 18 is the transverse displacement of the mid point of the beam in both time and frequency domains. Clearly, the excitation favors the fifth linear mode (symmetric mode of frequency equal to 1055 Hz) and its response is significantly nonlinear leading to the broad response peak seen in Fig. 18. Note as well the presence of sharper peaks at smaller energy levels associated with the first and third modes which are out of band but are excited by the nonlinear interaction of the modes. The introduction of uncertainty in the linear and nonlinear stiffness tensors leads to the spectrum plot of Fig. 19. Surprisingly, it is found that the dominant peak is quite robust but that a very large uncertainty band occurs in conjunction with the first mode. In fact, the 95th percentile of the spectrum at this first peak is at the same energy level than that of the dominant peak. Thus, uncertainty on this narrowband response manifest itself mostly by a potentially dramatic increase in the component of response associated with the first linear mode.

SUMMARY

The focus of this investigation has been on the formulation of a general methodology for the consideration of both data and model uncertainty in the modeling of geometrically nonlinear dynamic systems. It was argued first that the most appropriate framework for the inclusion of model uncertainty is in terms of reduced order models of the system, especially those which are build from a deterministic basis, e.g. the linear modes of the mean model.

On this basis, a comprehensive analysis was undertaken to clarify the derivation of such reduced order models, first from the governing equations of a linearly elastic continuum. An important aspects of this effort was to highlight the fundamental properties of the various tensors involved in the reduced order model as these properties will have to be satisfied for every realization of the uncertain reduced order model. Symmetry properties of the mass and the three stiffness tensors were first stated. Next, the positive definiteness of the stiffness tensors $\underline{\underline{K}}^{(1)}$ and $\underline{\underline{K}}^{(3)}$ was recognized but this statement was shown to be resulting from a stronger positive definiteness property that involves all three stiffness tensors, i.e. of the matrix $\underline{\underline{K}}_B$ of Eq. (26). The derivation of a reduced order model of a geometrically nonlinear system from a computational model (e.g. finite element model) of it was also addressed and a recently devised approach (the STEP algorithm) was reviewed in details. It was finally noted that a complete reduced order model should also include the characterization of the stress field and this task was also achieved.

The stochastic modeling of uncertainty (data and model) within the context of the reduced order model was considered next. It was highlighted that such a modeling cannot be achieved in an ad-hoc manner but rather should be deep rooted in stochastic mechanics to achieve the generality and accuracy desired. To this end and following recent work in this area, a nonparametric approach was adopted in which the joint distribution of the coefficients of the reduced order model was not postulated but rather derived according to the maximum entropy principle under the constraints of symmetry and positive definiteness demonstrated earlier. The consideration of uncertainty in mass, damping, "structural" stiffness, and temperature-related stiffness terms according to this nonparametric approach was described in detail and was found to be computationally advantageous (owing to expedient algorithms for the simulation of samples of the reduced order model coefficients) and appealing in practical applications (because it requires only one measure of dispersion to characterize the uncertainty). Further, the nonparametric

approach leads to reduced order models in which all coefficients are random and are generally dependent on each other, as might be expected from an uncertain system.

A slender beam was finally considered to exemplify the methodology presented and its specific mean reduced order model was first derived by the STEP algorithm from a full finite element model. Next, uncertainty in mass, damping, "structural" stiffness, and temperature-related stiffness terms were all considered one at a time to demonstrate the application of the nonparametric methodology and compare the effects of these different types of uncertainty on both displacements and stresses inside the beam. These results were found to be in good agreement with physical expectations.

REFERENCES
1. Ewins, D.J., "The Effects of Detuning upon the Forced Vibrations of Bladed Disks," *Journal of Sound and Vibration,* Vol. 9, pp. 65-79, 1969.
2. Ghanem, R., and Spanos, P.D., *Stochastic Finite Elements: A Spectral Approach*, Springer-Verlag, New York, 1991.
3. Soize, C., "A Nonparametric Model of Random Uncertainties on Reduced Matrix Model in Structural Dynamics," *Probabilistic Engineering Mechanics*, Vol. 15, No. 3, pp. 277-294, 2000.
4. Soize, C., "Maximum Entropy Approach for Modeling Random Uncertainties in Transient Elastodynamics," *Journal of the Acoustical Society of America*, Vol. 109, No. 5, pp. 1979-1996, 2001.
5. Soize, C., "Random Matrix Theory for Modeling Uncertainties in Computational Mechanics," *Computer Methods in Applied Mechanics and Engineering*, Vol. 194, pp. 1333-1366, 2005.
6. Soize, C., "Probabilistic Models for Computational Stochastic Mechanics and Applications," *Proceedings of the 9th International Conference on Structural Safety and Reliability ICOSSAR'05*, Rome, Italy, 19-23 June 2005, Augusti, G., Schueller, G.I., and Ciampoli, M., (Eds). Millpress, Rotterdam, Netherlands, pp.23-42.
7. Muravyov, A.A., and Rizzi, S.A., "Determination of Nonlinear Stiffness with Application to Random Vibration of Geometrically Nonlinear Structures," *Computers and Structures*, Vol. 81, No. 15, pp. 1513–1523, 2003.
8. Mignolet, M.P., Radu, A.G., and Gao, X., "Validation of Reduced Order Modeling for the Prediction of the Response and Fatigue Life of Panels Subjected to Thermo-Acoustic Effects", *Proceedings of the 8th International Conference on Recent Advances in Structural Dynamics*, Southampton, United Kingdom, Jul. 14-16, 2003.
9. Radu, A., G., Yang, B., Kim, K., and Mignolet, M.P., "Prediction of the Dynamic Response and Fatigue Life of Panels Subjected to Thermo-Acoustic Loading," *Proceedings of the 45th Structures, Structural Dynamics, and Materials Conference*, Palm Springs, California, Apr. 19-22, 2004.
10. Hollkamp, J.J., Gordon, R.W., and Spottswood, S.M., "Nonlinear Modal Models for Sonic Fatigue Response Prediction: A Comparison of Methods," *Journal of Sound and Vibration*, Vol. 284, No. 3-5, pp. 1145-1163, 2005.
11. Fung, Y.C., and Tong, P., *Classical and Computational Solid Mechanics*, World Scientific, River Edge, New Jersey, 2001.
12. Bonet, J., and Wood, R.D., *Nonlinear Continuum Mechanics for Finite Element Analysis*, Cambridge University Press, Cambridge, 1997.
13. Devroye, L., *Non-Uniform Random Variate Generation*, Springer Verlag, New York, 1986.
14. Bathe, K.-J., and Wilson, E.L., *Numerical Methods in Finite Element Analysis*, Prentice-Hall, Englewood Cliffs, New Jersey, 1976.
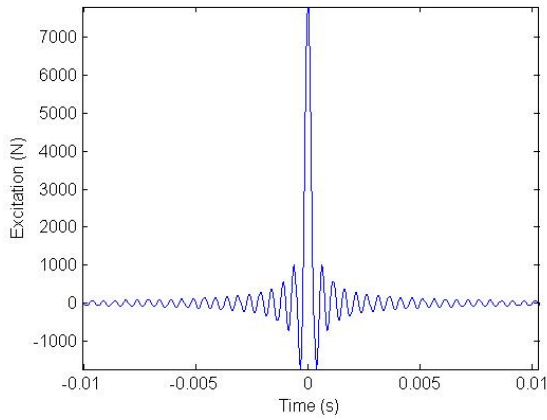
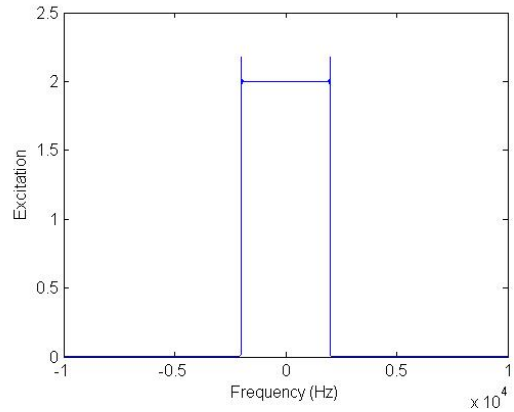Figure 1. Time history of the force.
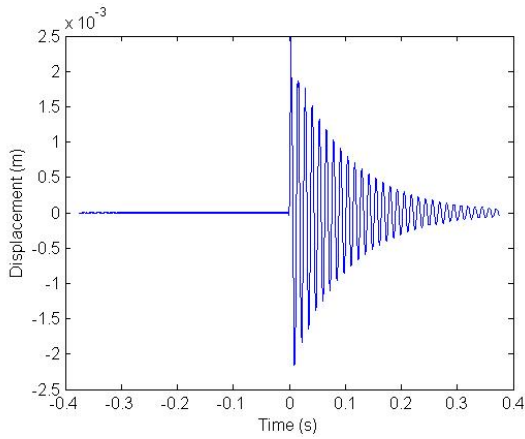

Figure 2. Spectral content of the force.

Figure 3. Transverse displacement of the middle of the beam (linear mean model) as a function of time.
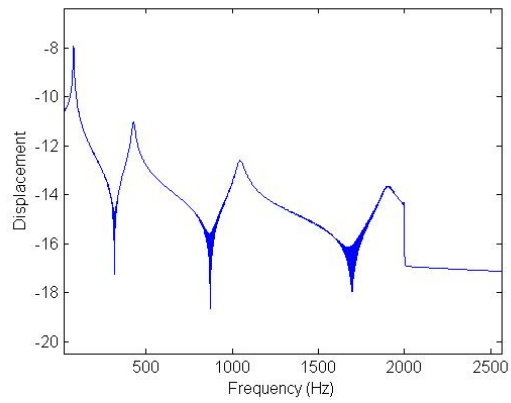

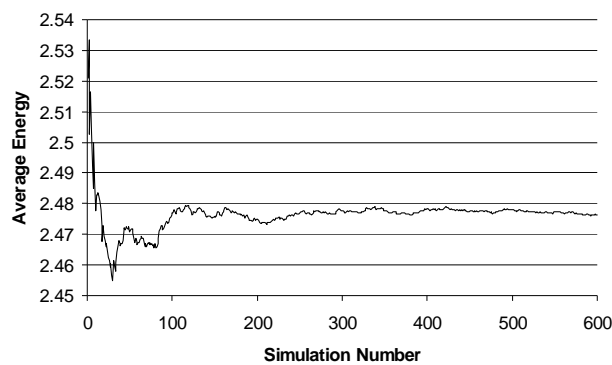Figure 4. Transverse displacement of the middle of the beam (linear mean model) as a function of frequency.

Figure 5. Evolution of the estimate of the mean modal signal energy as a function of the number of samples, linear reduced order model
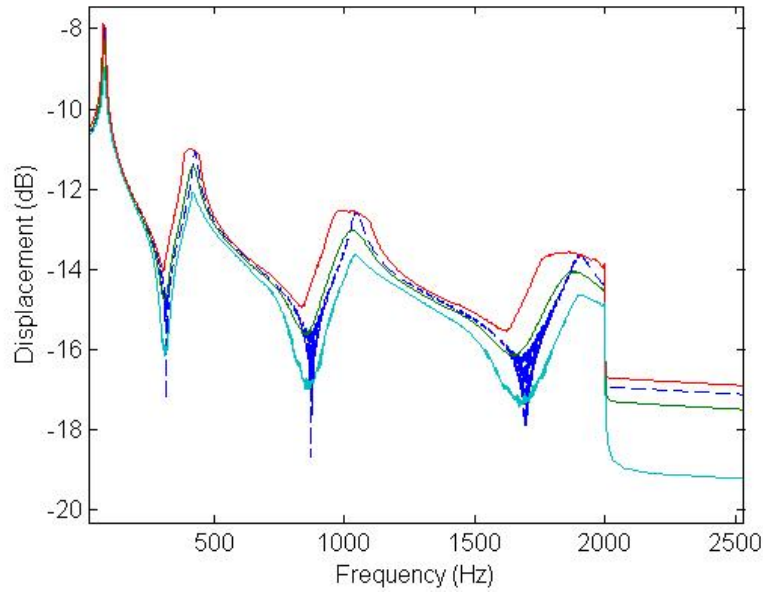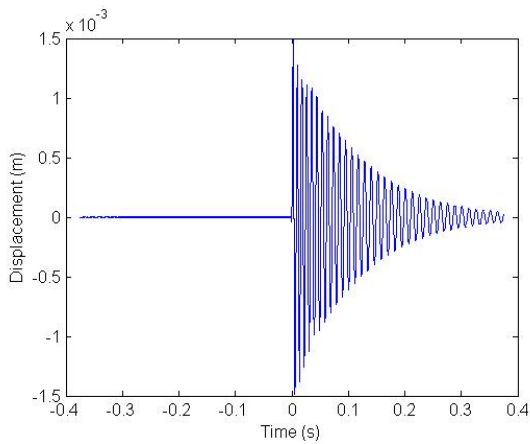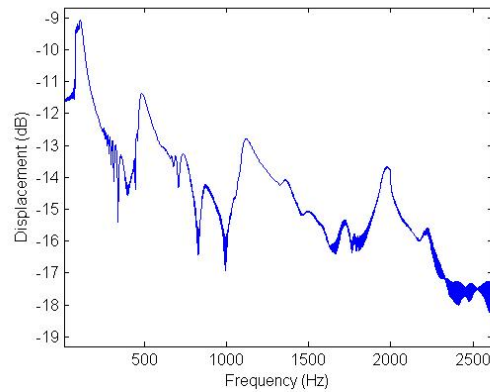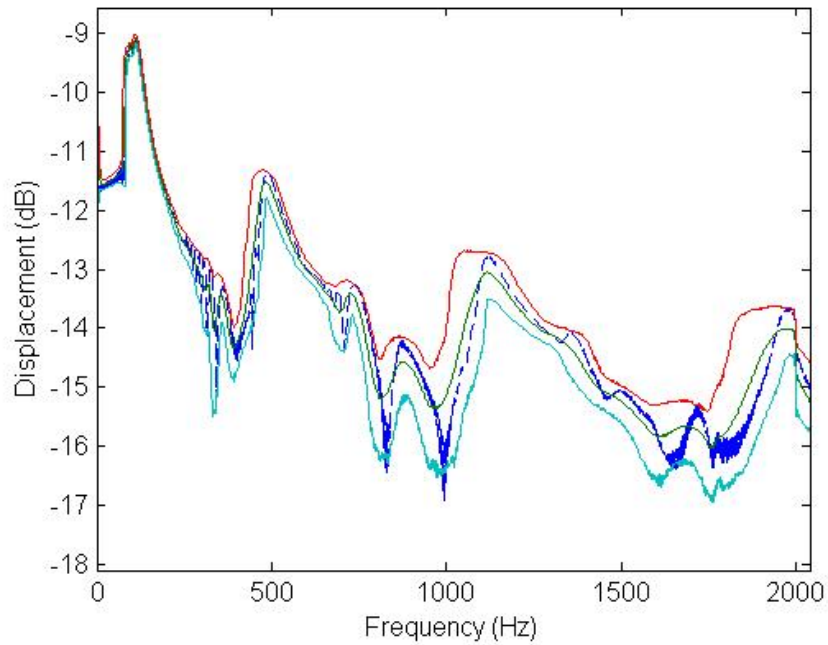
Figure 6. Transverse displacement of the middle of the random linear beam as a function of frequency. Mean (green line), 5th (light blue), and 95th (red line) percentile of the spectrum and spectrum of the mean model (dashed lines). Excitation of Figs 1 and 2.

Figure 7. Transverse displacement of the middle of the beam (nonlinear mean model) as a function of time.

Figure 8. Transverse displacement of the middle of the beam (nonlinear mean model) as a function of frequency.

Figure 9. Transverse displacement of the middle of the random nonlinear beam as a function of frequency. Mean (green line), 5th (light blue), and 95th (red line) percentile of the spectrum and spectrum of the mean model (dashed lines). Uncertainty on stiffness. Excitation of Figs 1 and 2 and mean model response of Figs 7 and 8.
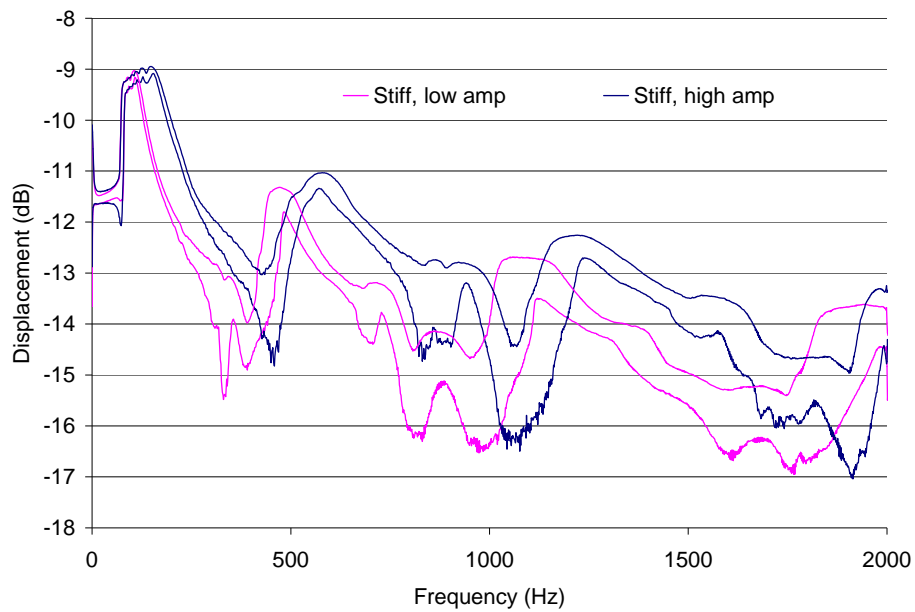

Figure 10. 5th -95th percentile bands of the spectrum of the transverse beam displacement at its middle at two response levels. Uncertainty on stiffness.
"Stiff, low amp": Excitation of Figs 1 and 2 and mean model response of Figs 7 and 8. "Stiff, high amp": Excitation of Figs 1 and 2 x 2.25.
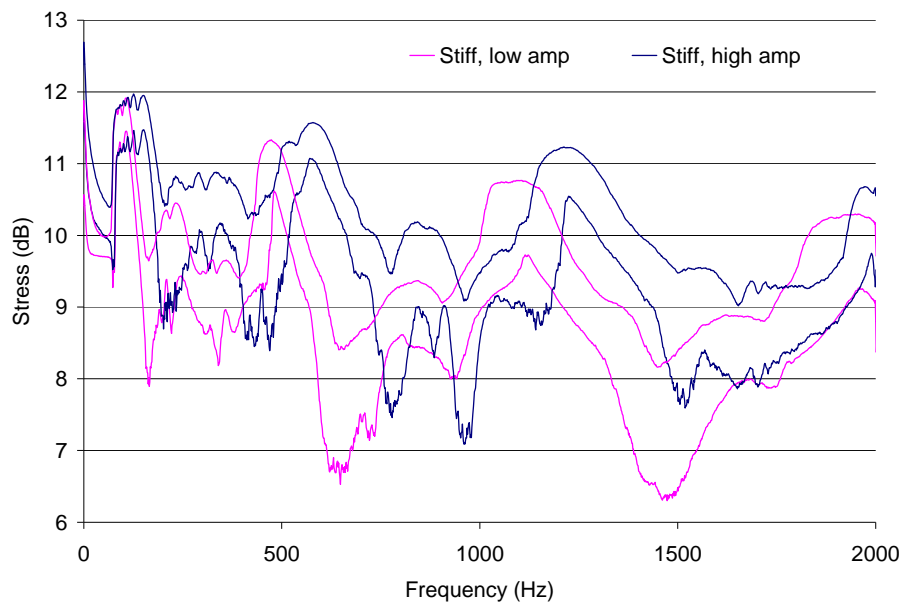
Figure 11. 5th -95th percentile bands of the spectrum of the stress σ_x at the beam middle at two response levels. Uncertainty on stiffness. "Stiff, low amp": Excitation of Figs 1 and 2 and mean model response of Figs 7 and 8. "Stiff, high amp": Excitation of Figs 1 and 2 x 2.25.
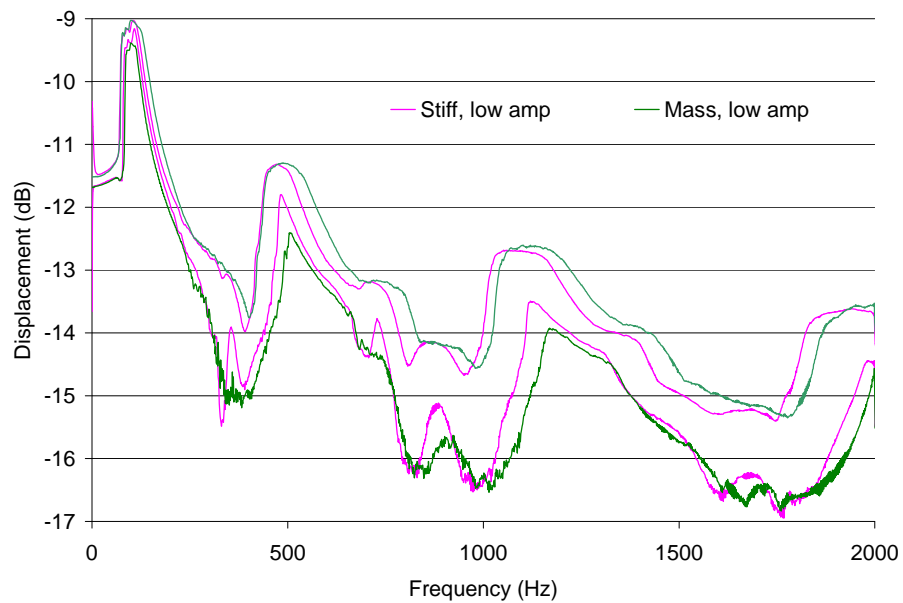
Figure 12. 5th -95th percentile bands of the spectrum of the transverse beam displacement at its middle for the excitation of Figs 1 and 2 and mean model response of Figs 7 and 8. "Stiff, low amp": uncertainty on stiffnesses only, "Mass, low amp": uncertainty on masses only.
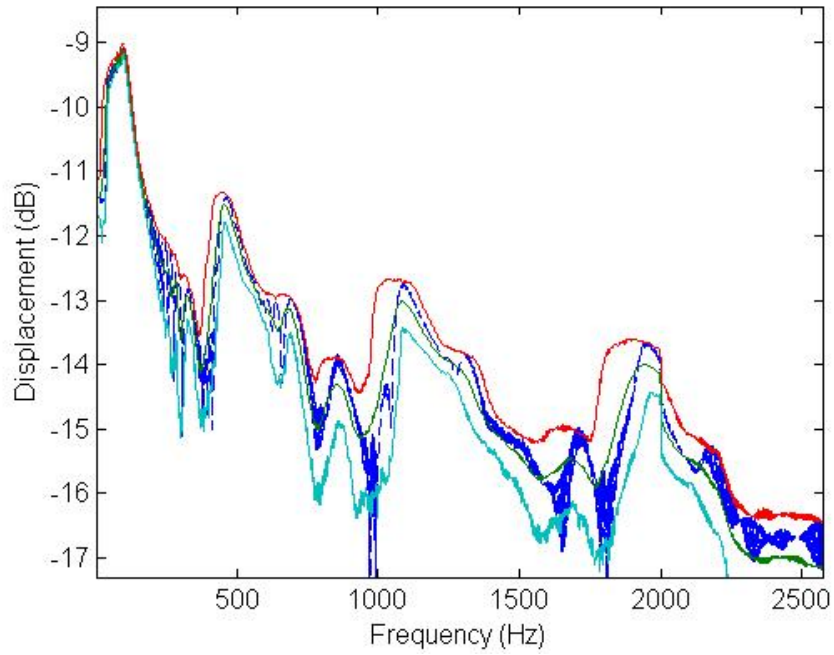
Figure 13. Transverse displacement of the middle of the random nonlinear beam as a function of frequency. Mean (green line), 5th (light blue), and 95th (red line) percentile of the spectrum and spectrum of the mean model (dashed lines).
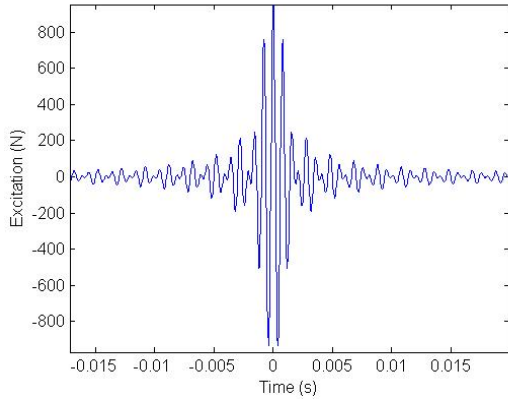Excitation of Figs 1 and 2 with T=1.25°C. Uncertainty on structural stiffness tensors.
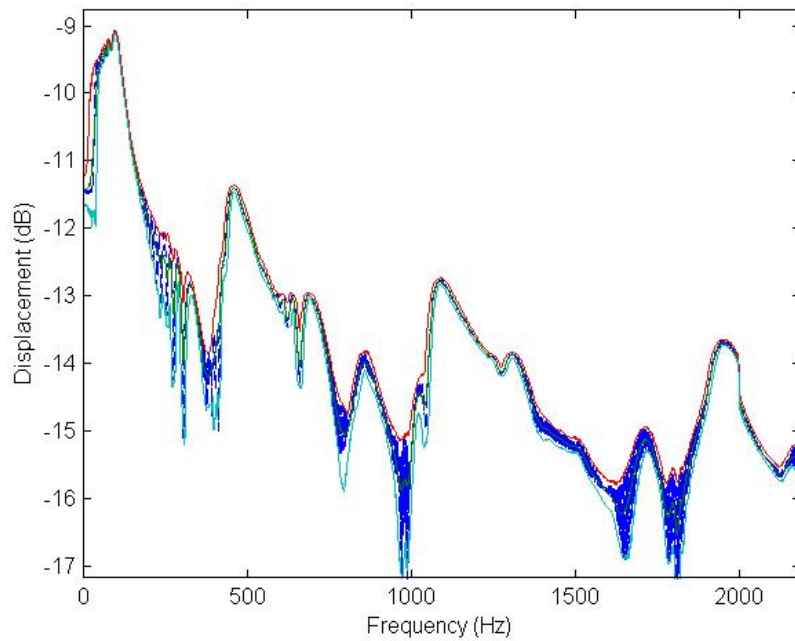
Figure 14. Transverse displacement of the middle of the random nonlinear beam as a function of frequency. Mean (green line), 5th (light blue), and 95th (red line) percentile of the spectrum and spectrum of the mean model (dashed lines).
Excitation of Figs 1 and 2 with T=1.25°C. Uncertainty on thermal stiffness matrix.
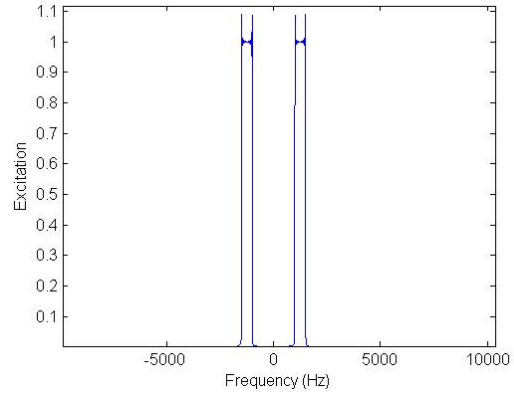
Figure 15. Time history of the narrowband force.

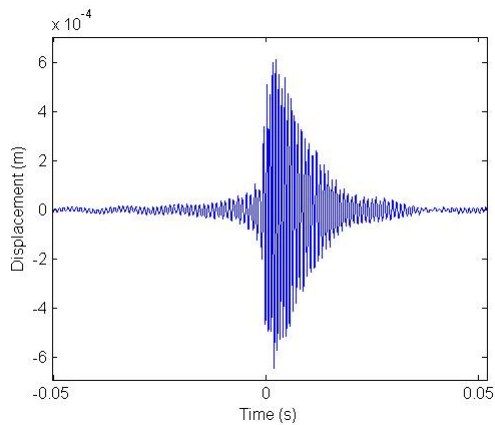Figure 16. Frequency content of the narrowband force.

Figure 17. Transverse displacement of the middle of the beam subjected to the narrowband force, as a function of time.
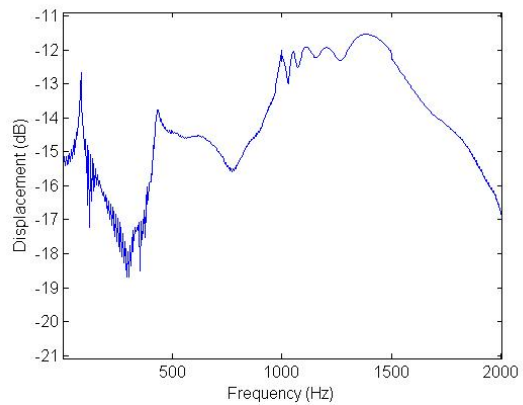

Figure 18. Transverse displacement of the middle of the beam subjected to the narrowband force, as a function of frequency.
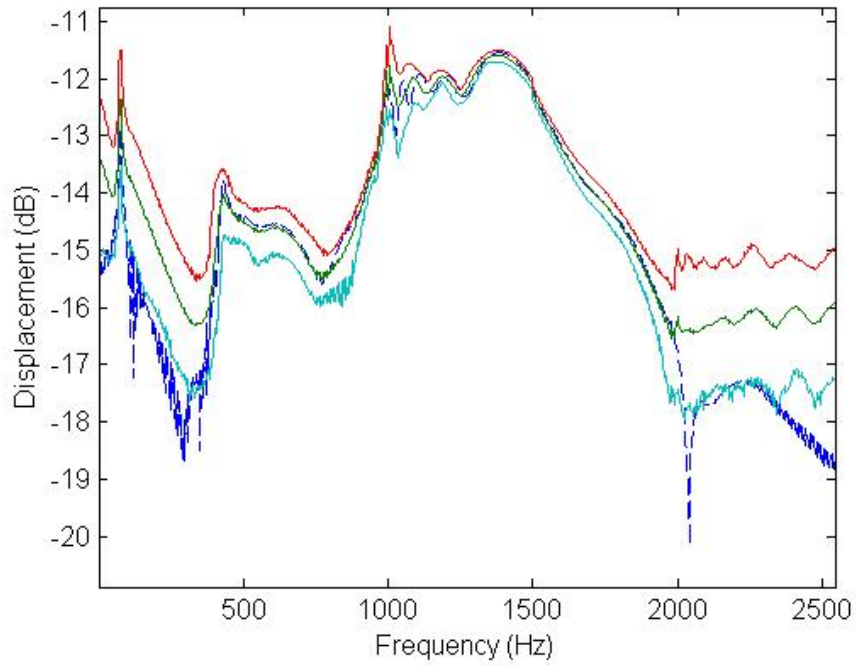
Figure 19. Transverse displacement of the middle of the random nonlinear beam as a function of frequency. Mean (green line), 5th (light blue), and 95th (red line) percentile of the spectrum and spectrum of the mean model (dashed lines).
Excitation of Figs 15 and 16. Uncertainty on stiffness.